

Precise control of the coupling coefficient through destructive interference in silicon waveguide Bragg gratings

Xu Wang,^{1,2,*} Yun Wang,¹ Jonas Flueckiger,¹ Richard Bojko,³ Amy Liu,² Adam Reid,² James Pond,² Nicolas A. F. Jaeger,¹ and Lukas Chrostowski¹

¹Department of Electrical and Computer Engineering, University of British Columbia, Vancouver, BC V6T 1Z4, Canada

²Lumerical Solutions, Vancouver, BC V6E 3L2, Canada

³Washington Nanofabrication Facility, University of Washington, Seattle, Washington 98195, USA

*Corresponding author: xuw@ece.ubc.ca

Received May 28, 2014; revised July 27, 2014; accepted August 18, 2014;
posted August 22, 2014 (Doc. ID 212993); published September 17, 2014

We present waveguide Bragg gratings with misaligned sidewall corrugations on a silicon-on-insulator platform. The grating strength can be tuned by varying the misalignment between the corrugations on the two sidewalls. This approach allows for a wide range of grating coupling coefficients to be achieved with precise control, and substantially reduces the effects of quantization error due to the finite mask grid size. The experimental results are in very good agreement with simulations using the finite-difference time-domain (FDTD) method. © 2014 Optical Society of America

OCIS codes: (050.2770) Gratings; (130.3120) Integrated optics devices; (230.7370) Waveguides.
<http://dx.doi.org/10.1364/OL.39.005519>

Silicon photonics is a promising technology for photonic integrated circuits, and Bragg gratings are a key component in this technology. Over the last few years, various grating structures and devices have been demonstrated, such as uniform gratings [1], apodized gratings [2], sampled gratings [3], high- Q phase-shifted grating cavities [4], and grating-assisted contra-directional couplers [5]. Their applications are also being increasingly developed for optical communications [6], biosensing [7], microwave photonics signal processing [8], etc. While significant efforts and progress have been made in this field, many challenges still exist. Since silicon waveguide Bragg gratings are usually based on small physical corrugations, their performance highly depends on the fabrication process and can be easily affected by fabrication imperfections, such as optical lithography smoothing effect [9], silicon thickness variations [4], and quantization errors due to the finite mask grid size (e.g., 1, 5, and 6 nm). Strip waveguides are often used for relatively broadband gratings. As will be discussed shortly, a 500 nm \times 220 nm strip waveguide with 50 nm sidewall corrugations can result in a bandwidth of about 25 nm, and a bandwidth of less than 1 nm would require corrugations that are challenging to manufacture. However, numerous applications require narrow bandwidths. To reduce the bandwidth while keeping the minimum feature size reasonable, several approaches have been proposed, such as cladding-modulated gratings [10] and rib waveguide gratings [1,11]. The former approach uses weakly coupled pillars outside of the core waveguide; however, it is challenging to realize isolated pillars using optical lithography. The latter has shown bandwidths narrower than 1 nm but requires two etch steps.

In this Letter, we present Bragg gratings based on a strip waveguide where we intentionally misalign the corrugations on the two sidewalls, as illustrated in Fig. 1(a). This structure can be broken down into two individual gratings with a phase offset. When there is no misalignment, the

two gratings are in phase, and all the reflections interfere constructively at the Bragg wavelength. When there is a misalignment, the interference becomes less constructive, and therefore, the grating strength becomes weaker. In the extreme case where the two gratings are completely out of phase, destructive interference occurs, and the whole structure behaves like a wavy waveguide with essentially no reflection. A similar concept has been implemented in grating-assisted contra-directional couplers to suppress the back reflections [12]. The superposition of two gratings can also be used to achieve apodized gratings [2,13]. Note that all the corrugations here have the same period. This differs from the multi-period grating concept where, even though misalignment exists, the multiple gratings do not interfere with each other because they operate at different wavelengths [4,14].

Figure 1(b) shows the waveguide cross section, along with the electric field intensity profile of the first mode that shows quasi-transverse-electric polarization. The silicon waveguide layer has a thickness of 220 nm and

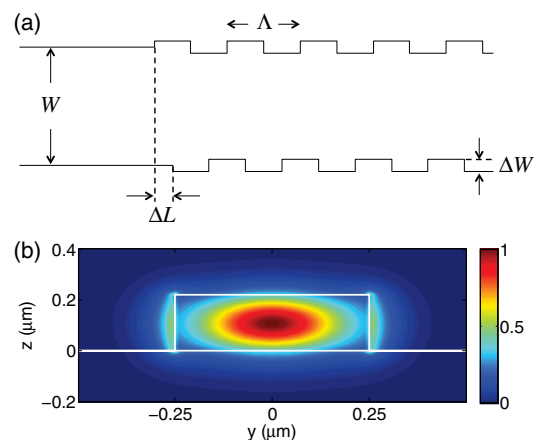


Fig. 1. (a) Top view grating schematic. (b) Waveguide cross section and mode profile (electric field intensity).

is sandwiched between the buried oxide layer and upper cladding of air. The average waveguide width (W) and corrugation width (ΔW) are designed to be 500 nm and 50 nm, respectively. The grating period (Λ) is 324 nm, with a duty cycle of 50%. The number of grating periods is 284 (i.e., corresponding to a grating length of about 92 μm). The misalignment (ΔL) is varied from 0 to 162 nm (i.e., completely in phase to completely out of phase). The devices were fabricated using electron-beam lithography with a 6-nm grid spacing, as described in [15]. The scanning electron microscope (SEM) images of the fabricated gratings are shown in Fig. 2.

The interaction of the grating with the optical mode, or the grating strength, is often described by the coupling coefficient (κ), which is the magnitude of the coupling between the forward and backward propagating modes. As mentioned above, we can divide the structure into two individual gratings and write the effective coupling coefficient as:

$$\kappa = \left| \frac{\kappa_0}{2} + \frac{\kappa_0}{2} \exp(i \cdot 2\pi\Delta L/\Lambda) \right| = \kappa_0 \cos\left(\frac{\pi\Delta L}{\Lambda}\right), \quad (1)$$

where κ_0 is the coupling coefficient for the grating with no misalignment (i.e., $\Delta L = 0$), and $2\pi\Delta L/\Lambda$ is the phase offset between the two grating components. In order to better understand this concept, we performed 3D finite-difference time-domain (FDTD) simulations using Lumerical FDTD Solutions [16]. Figure 3 shows the top view electric field distributions as light travels from left to right. When the misalignment is zero, light is strongly reflected back, and the field decays exponentially [4]. When the misalignment is half the grating period, light transmits through without reflection. In these FDTD simulations, the mesh size must be sufficiently fine to resolve the small sidewall corrugations, and the simulation time must be long enough for the electromagnetic fields to decay. Therefore, the FDTD simulation of the whole structure is computationally intensive. If the grating is very weak and long, it can be impractical to run the simulation to get accurate frequency-domain results. In this work, we investigate a more efficient FDTD approach, where we consider an infinitely long Bragg grating and simulate only one unit cell using Bloch boundary conditions [16]. This is a well-known method for calculating the band structure of periodic structures such as photonic crystal waveguides [17]. Bloch boundaries are used along the propagation direction x , and the Fourier transform of the time domain signals are used to locate the band

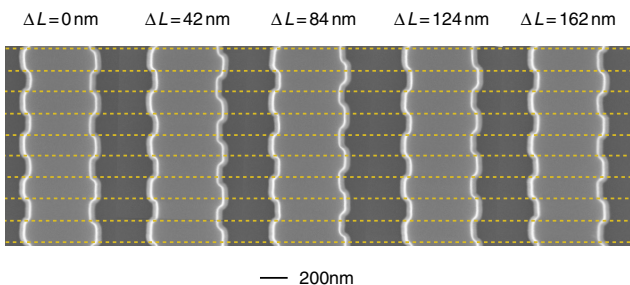


Fig. 2. SEM images of the fabricated gratings with various misalignment lengths.

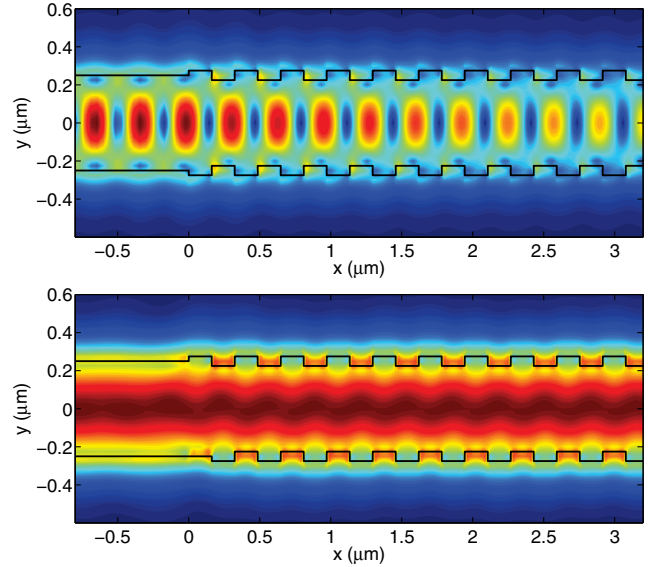


Fig. 3. Electric field distributions with light incident from the left for gratings with (top): $\Delta L = 0$, and (bottom): $\Delta L = 162$ nm, both at the Bragg wavelength for the design of $\Delta L = 0$. The field is recorded at the middle of the silicon waveguide in the vertical direction, i.e., corresponding to the plane of $z = 110$ nm in Fig. 1(b).

gap, i.e., the center wavelength (λ_0) and the bandwidth ($\Delta\lambda$), of the grating, as shown in Fig. 4. Based on these results, the coupling coefficient can be calculated as [18]:

$$\kappa = \pi n_g \Delta\lambda / \lambda_0^2, \quad (2)$$

where n_g is the group index. As κ represents the amount of reflection per unit length [19] or the field attenuation constant for the forward propagating mode, we can also obtain Eq. (2) using the definition of the intrinsic quality factor from [20] for an infinitely long grating:

$$Q = \frac{\omega_0}{c} \cdot \frac{n_g}{\alpha} = \frac{2\pi}{\lambda_0} \cdot \frac{n_g}{2\kappa} = \frac{\lambda_0}{\Delta\lambda}, \quad (3)$$

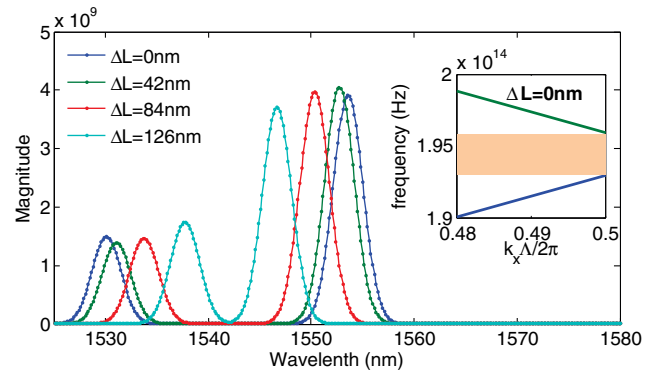


Fig. 4. Fourier transform (magnitude) of the time domain signals from FDTD simulations of one grating cell using Bloch boundary conditions. The two resonant peaks correspond to the band edges at the $k_x = \pi/\Lambda$ point, and the wavelength range between the two peaks corresponds to the band gap in which there are no propagating solutions. Inset: band structure for $\Delta L = 0$ nm.

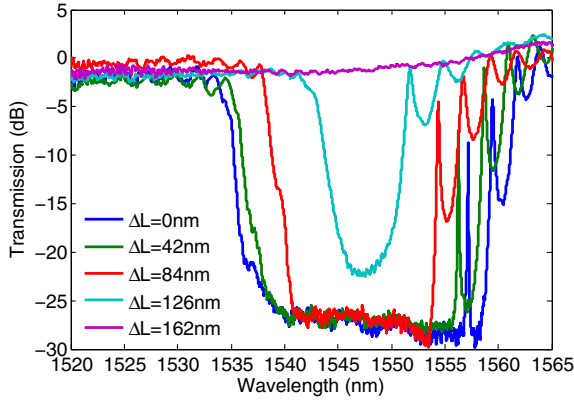


Fig. 5. Measured transmission spectra for gratings with different misalignment lengths. Note that the cut-off of the stop band between -25 dB and -30 dB was due to the source spontaneous emission of the tunable laser used for the measurement [4].

where ω_0 is the resonant frequency, and $\alpha = 2\kappa$ is the intensity attenuation constant. Even though the result of this simulation is only valid for an infinitely long grating, this FDTD technique is very useful for predicting κ and how it is affected by geometric variations such as changing ΔL or ΔW .

The measurement of the chip was performed on an automated probe station [21]. Figure 5 shows the normalized transmission spectra of the gratings. When ΔL is zero, the measured bandwidth is about 25 nm. As ΔL increases, the stop band becomes narrower. When ΔL is $\Lambda/2$, the stop band disappears and the spectrum becomes a straight line. The coupling coefficients can be extracted from these spectra using the method described in [4], and are shown as the open blue squares in Fig. 6. The simulated coupling coefficients based on Fig. 4 and Eq. (2) are also shown in Fig. 6. The agreement between the experimental data and the FDTD simulation is excellent. The theoretical relationship between κ and ΔL , as described in Eq. (1), is also verified.

We also compare this grating concept with the conventional approach of adjusting the grating strength by

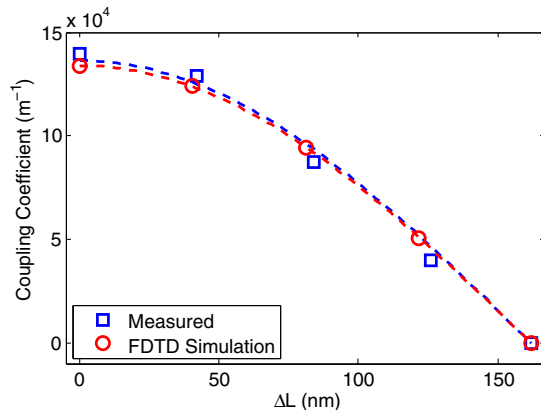


Fig. 6. Coupling coefficient as a function of misalignment length for gratings with a fixed corrugation width ($\Delta W = 50$ nm). The blue open squares come from the measurement data in Fig. 5. The red open squares come from the FDTD simulation results in Fig. 4. The dashed curves are the fits using the formula in Eq. (1).

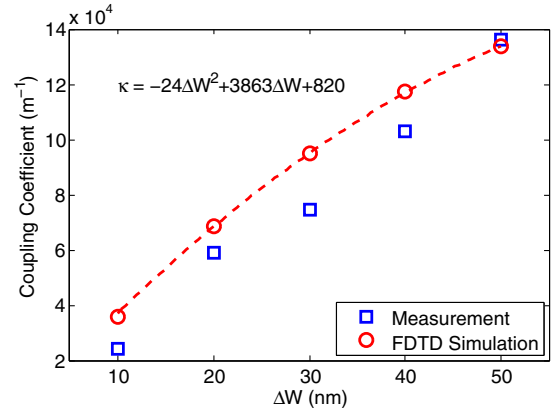


Fig. 7. Coupling coefficient as a function of corrugation width for gratings with no misalignment ($\Delta L = 0$).

varying the corrugation size. Specifically, we keep ΔL to be zero and vary ΔW from 10 to 50 nm. As shown in Fig. 7, the simulated coupling coefficient can be fitted by a second-order polynomial of ΔW . The difference between simulation and measurement is more pronounced than that in Fig. 6, indicating that it is more sensitive to fabrication errors.

By varying both ΔW and ΔL , we can achieve various κ values, as shown in Fig. 8. In reality, however, there are quantization errors due to the finite mask grid size (6 nm in this case). To evaluate the quantization errors introduced by the different techniques, we define the maximum error as half the difference between two consecutive achievable κ values, and the results are shown in Fig. 9. The ΔW -only technique shows significant quantization errors. Reducing the grid size (e.g., to 2 nm) can reduce the quantization effect but at the expense of increasing the writing time and cost. The ΔL -only technique shows smaller and nonuniform errors—large κ values are less sensitive to ΔL than small κ values, which can be understood by taking the derivative of Eq. (1) with respect to ΔL . By combining the two techniques, very fine-resolution κ values can be obtained.

Note that if the same designs were fabricated using optical lithography, the corrugations would be greatly smoothed and the grating strength would be much weaker [9]. Furthermore, for designs with varied grating strength (e.g., apodized gratings), one of the important benefits of the ΔL approach is that the lithography

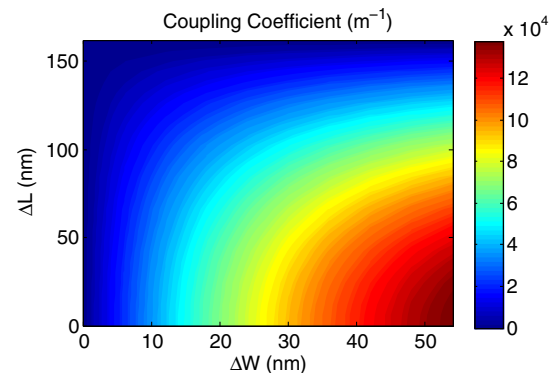


Fig. 8. Contour plot of κ versus ΔW and ΔL , based on the curve fitting results in Fig. 7 and Eq. (1).

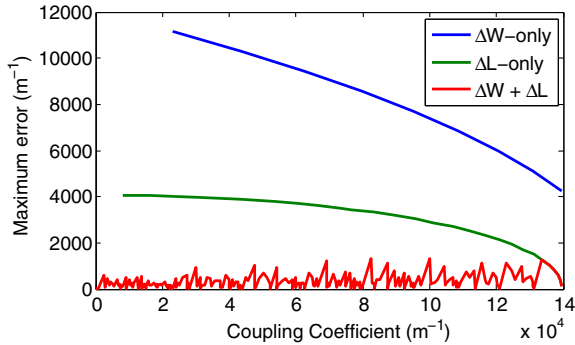


Fig. 9. Quantization errors using different techniques. For each technique, we sort all the κ values that can be achieved with the 6-nm grid (i.e., discrete data points in Fig. 8) and then calculate the differences between adjacent κ values. The maximum error occurs at the midpoint between adjacent κ values and equals to half the difference.

smoothing effects only need to be calibrated once for a particular ΔW , yet the approach allows for arbitrary grating strength ranging from 0 to the maximum achievable κ for the particular ΔW . This is in contrast to modulating ΔW to create an arbitrary grating strength profile, where each ΔW needs to be carefully calibrated for lithography to obtain the correct κ and average effective index values, thus requiring a dramatically more complicated design process.

In summary, we have demonstrated integrated waveguide Bragg gratings with misaligned sidewall corrugations that allow for precise control of the coupling coefficient. We have shown that the misalignment's contribution to the coupling coefficient is a cosine function of the phase offset, confirmed by both experimental results and numerical modeling. This approach adds another degree of flexibility to grating designs and considerably reduces the effects of quantization errors, making it attractive for many complex grating devices.

References

1. X. Wang, W. Shi, H. Yun, S. Grist, N. A. F. Jaeger, and L. Chrostowski, *Opt. Express* **20**, 15547 (2012).
2. A. Simard, N. Belhadj, Y. Painchaud, and S. LaRochelle, *IEEE Photon. Technol. Lett.* **24**, 1033 (2012).
3. X. Wang, W. Shi, R. Vafaei, N. A. F. Jaeger, and L. Chrostowski, *IEEE Photon. Technol. Lett.* **23**, 290 (2011).
4. X. Wang, "Silicon photonic waveguide Bragg gratings," Ph.D. thesis (University of British Columbia, 2013).
5. W. Shi, X. Wang, C. Lin, H. Yun, Y. Liu, T. Baehr-Jones, M. Hochberg, N. A. F. Jaeger, and L. Chrostowski, *Opt. Express* **21**, 3633 (2013).
6. W. Shi, V. Veerasubramanian, D. V. Plant, N. A. F. Jaeger, and L. Chrostowski, *Proc. SPIE* **9010**, 90100F (2014).
7. X. Wang, J. Flueckiger, S. Schmidt, S. Grist, S. T. Fard, J. Kirk, M. Doerfler, K. C. Cheung, D. M. Ratner, and L. Chrostowski, *J. Biophotonics* **6**, 821 (2013).
8. M. Burla, L. R. Cortés, M. Li, X. Wang, L. Chrostowski, and J. Azaña, *Opt. Express* **21**, 25120 (2013).
9. X. Wang, W. Shi, M. Hochberg, K. Adam, E. Schelew, J. F. Young, N. A. F. Jaeger, and L. Chrostowski, in *IEEE Conference on Group IV Photonics* (IEEE, 2012), pp. 288–290.
10. D. T. H. Tan, K. Ikeda, and Y. Fainman, *Opt. Lett.* **34**, 1357 (2009).
11. G. Jiang, R. Chen, Q. Zhou, J. Yang, M. Wang, and X. Jiang, *IEEE Photon. Technol. Lett.* **23**, 6 (2011).
12. W. Shi, H. Yun, C. Lin, M. Greenberg, X. Wang, Y. Wang, S. T. Fard, J. Flueckiger, N. A. F. Jaeger, and L. Chrostowski, *Opt. Express* **21**, 6733 (2013).
13. C. M. Greiner, D. Iazikov, T. W. Mossberg, B. McGinnis, R. Narevich, and A. Ticknor, *Proc. SPIE* **6896**, 68960G (2008).
14. X. Wang, H. Yun, N. Jaeger, and L. Chrostowski, in *IEEE Photonic Conference* (IEEE, 2013), pp. 442–443.
15. R. J. Bojko, J. Li, L. He, T. Baehr-Jones, M. Hochberg, and Y. Aida, *J. Vac. Sci. Technol. B* **29**, 06F309 (2011).
16. Lumerical Solutions, Inc., <https://www.lumerical.com/>.
17. M. Loncar, T. Doll, J. Vuckovic, and A. Scherer, *J. Lightwave Technol.* **18**, 1402 (2000).
18. D. C. Flanders, H. Kogelnik, R. V. Schmidt, and C. V. Shank, *Appl. Phys. Lett.* **24**, 194 (1974).
19. J. Buus, M.-C. Amann, and D. J. Blumenthal, *Tunable Laser Diodes and Related Optical Sources*, 2nd ed. (Wiley, 2005).
20. L. Chrostowski, S. Grist, J. Flueckiger, W. Shi, X. Wang, E. Ouellet, H. Yun, M. Webb, B. Nie, Z. Liang, K. C. Cheung, S. A. Schmidt, D. M. Ratner, and N. A. F. Jaeger, *Proc. SPIE* **8236**, 823620 (2012).
21. L. Chrostowski and M. Hochberg, *Silicon Photonics Design* (Cambridge University, 2014).